IEEE JOURNAL OF OCEANIC ENGINEERING, VOL. 37, NO. 4, OCTOBER 2012

pp. 756-763

Digital Object Identifier 10.1109/JOE.2012.2204151

Ceramic Pressure-tight Housings for Ocean-bottom Seismometers Applicable to 11 km Water Depth

***Abstract*- Ceramics have some outstanding features that are necessary for pressure-tight housings, such as higher compressive strength, lower specific gravity, and higher resistance against corrosion. One promising application is pressure-tight housings for a free-fall pop-up Ocean-Bottom Seismometer (OBS). Ceramic pressure-tight housings can provide sufficient strength and buoyancy even at 11 km water depth. Nevertheless, tensile and bending strengths of ceramics are only a fraction of their compressive strength. For metals, they are almost equal. Therefore common design methods for pressure-tight housings are not directly applicable to ceramic pressure-tight housings. As described herein, we propose a new design method for ceramic pressure-tight housings, particularly a method of reinforcement of through-holes for underwater connectors. We also present detailed data that support the proposed design method.**

I. INTRODUCTION

Ceramics have higher compressive strength than many metals, as presented in Fig. 1. They also have lower specific gravity and they are not vulnerable to corrosion by seawater. Therefore, durable, light, pressure-tight ceramic housings can be produced, providing sufficient buoyancy and enabling operations even at 11 km water depth. When applied to underwater vehicles that need neutral buoyancy, they can reduce the need for expensive syntactic foam. However, tensile and bending strengths of ceramics are only a fraction of their compressive strengths, as presented in Fig. 1, although they are almost identical in the case of metals. Therefore common design methods for pressure-tight housings of metals are not directly applicable to ceramic pressure-tight housings.

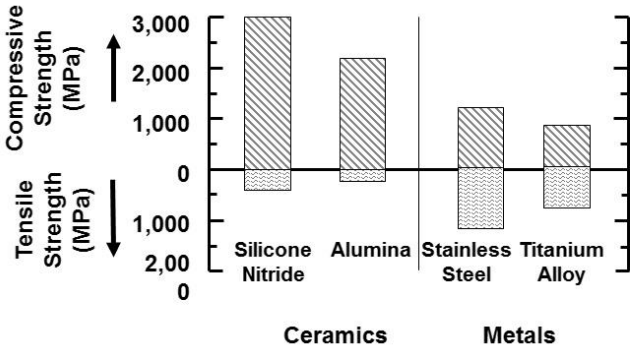

Fig. 1. Typical ceramic and metal strengths.
Silicone Nitride Ceramic: SN240 by Kyocera
Alumina Ceramic: A479 by Kyocera
Stainless Steel: SUS630-H900
Titanium Alloy: Ti-6Al-4V
The compressive strength of SN240 was the averaged compressive strength of ten test pieces following JIS R608 testing method.

Stachiw [1], through vigorous studies of ceramic pressure-tight housings from 1961, laid the foundation for the development of 3.6-inch and 10-inch ceramic flotation spheres for deep-sea applications [2], [3], and a ceramic pressure-tight housing for the 11 km water depth hybrid underwater vehicle NERUS [4]. In Japan, Yano and Takagawa [5], [6] developed small ceramic sphere pressure-tight housings and studied their characteristics.

One issue to be addressed is reinforcement of through-holes for underwater connectors. Multiple through-holes are often necessary to electrically connect external devices to devices in the housings. Stress concentrations of twice normal levels are well known to appear around a through-hole on a thin infinite plane to which two orthogonal stresses are added parallel to the plane. It can be anticipated that a similar stress concentration appears around a through-hole on a sphere exposed to hydraulic pressure. This stress concentration is expected to have an important effect on the pressure tolerance of the housing. To address this issue, we increased the shell thickness around the through-hole to reduce stress. Proper reinforcement can reduce the stress concentration[7].

A promising application of ceramic pressure-tight housings is a free-fall pop-up Ocean Bottom Seismometer (OBS) such as that shown in Fig. 2. After deployment from a vessel, the free-fall pop-up OBS remains on the seafloor for several months, recording tremors using built-in recorders. When monitoring is completed, they detach ballast in

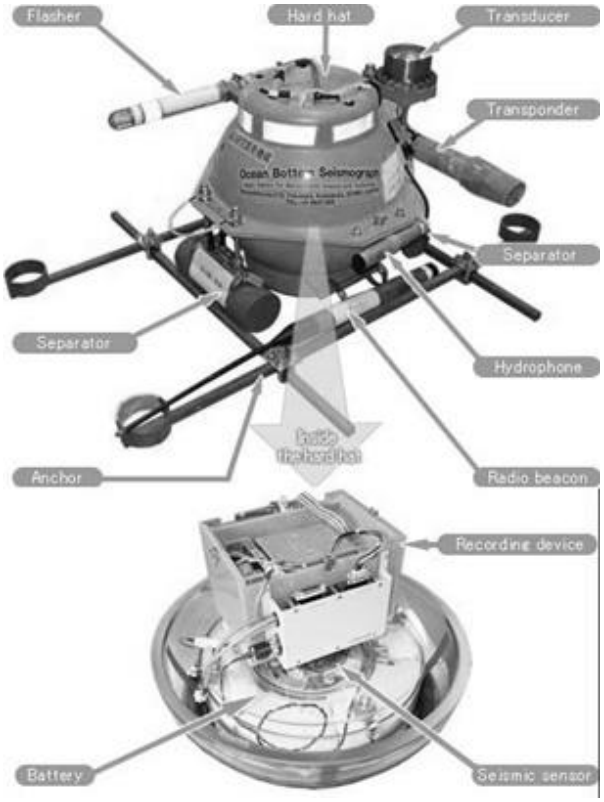

Fig. 2. Configuration of typical OBS.
(from http://www.nmeweb.jp/e/duties_tectonic_obs2.html#obs_hh)

response to acoustic commands sent from recovery vessels, at which time they ascend to the ocean surface. Housings must be sufficiently light to ensure their buoyancy. To date, 17-inch glass spheres have been used as pressure-tight housings for free-fall pop-up OBSs [8].

A glass sphere consists of two glass hemispheres. The coupling portion of the two hemispheres is sealed with self-bonding rubber. A three-axis seismometer, batteries and a recorder are mounted in the glass sphere. Other devices including an acoustic transponder, a hydrophone, a strobe light and a radio beacon are mounted outside of the glass sphere. The hydrophone is connected to the recorder in the glass sphere through a feed-through or an underwater connector on the glass sphere.

However, the maximum applicable depth of a 17-inch glass sphere is limited to about 6 km. The Japan Trench, where the catastrophic earthquake occurred on March 11, 2011, creating the devastating tsunami, is among those areas where seismic monitoring has not yet been conducted adequately because the maximum water depth of the Japan trench is about 8 km. That disaster demonstrated the importance of seismic monitoring on the seafloor at depths greater than 6 km. To extend the maximum operating depth of OBSs, we have developed small models of silicon-nitride ceramic pressure-tight housings for OBSs, as depicted in Fig. 3 [7], which are made of silicon-nitride ceramic. They can withstand hydraulic pressure of 110 MPa. Following the success of hydraulic

Fig. 3. Photograph of a small model of a ceramic pressure-tight housing for OBS.

pressure tests, we developed an actual-sized silicon-nitride ceramic pressure-tight housing (Fig. 4) and confirmed that it can withstand hydraulic pressure of 110 MPa [9]. Its diameter, mass, and volume are, respectively, 445 mm, 20.4 kg and 46.6 liters. These parameters are almost identical to those of conventional 17-inch glass spheres. We are now developing other devices that require an OBS of 11 km depth. We will deploy and test them on the deep seafloor in the near future to demonstrate their practicality.

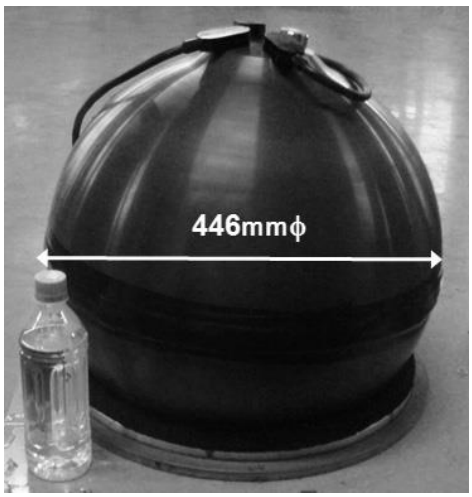

Fig. 4. Photograph of the ceramic pressure-tight housing designed for OBS. It can withstand hydraulic pressure of 110 MPa.

We have also developed small models of alumina ceramic pressure tight housings [9]. Although the compressive strength of alumina ceramic is about two-thirds that of silicon-nitride ceramic, its cost is much less than that of silicon-nitride ceramic. The maximum hydraulic pressure was set as 80 MPa. Test results show good characteristics against hydraulic pressure. The break-down hydraulic pressure was 172 MPa, which fairly coincided with the designed break-down pressure.

In this paper, we explain the pressure-tight ceramic housing design method. We also present detailed data supporting the design method. We have used finite element method (FEM) to evaluate the stress distribution on the ceramic housing and especially the stress concentration around the through-hole. We have assumed a design criterion

by which the product of a safety factor and the peak value of the minor principal stress do not exceed the uniaxial compressive strength.

First, stress concentrations were confirmed as appearing around the inner edge of through-holes and inner foot of the reinforcement. The effects of mesh size on the stress concentration were evaluated for selection of a suitable mesh size. Further analyses of many cases of reinforcement around through-holes revealed that a certain relation exists between the thickness of the reinforcement and the stress concentration. This relation is useful for the design of the reinforcement around the through-hole. Moreover, the effect of the reinforcement was found to have its own limitations. The stress concentration coefficient, defined as the ratio between the peak value of the minor principal stress and the hoop stress on the inner surface of the sphere, does not decrease below 1.12.

We also briefly present the results of hydraulic pressure tests.

This report is based on papers presented at OCEANS'10[7] and UT'11 + SSC'11[9].

II. FEM Analysis

A. Typical results of FEM analysis of a pressure-tight housing for use at 11 km water depth

Before making small models, we conducted FEM analyses to determine the best shape for reinforcement around through-holes. Multiple through-holes are needed to

accommodate underwater connectors and a vacuum port. For analyses, we assumed four through-holes. Table 1 presents the mechanical characteristics of silicon-nitride ceramic

Table 1 Mechanical characteristics of silicon-nitride ceramic and the alumina ceramic
The uniaxial compressive strengths are obtained by compression tests

Item	Unit	Silicon-nitride Ceramic (Kyocera SN240)	Alumina Ceramic (Kyocera A479)
Uniaxial Compressive Strength	MPa	3,000	2,160
Tensile Strength	MPa	726	166
Young's coefficient	GPa	300	360
Poison Ratio		0.28	0.23
Density	g/cm^3	3.3	3.8

and alumina ceramic. We used an I-DEAS 12 NX Series FEM analyzer.

Fig. 5 depicts the model used for FEM analysis of the pressure-tight hemisphere for the OBS of 11 km depth. We analyzed only 1/4 of the hemisphere, relying upon symmetry of the model.

Fig. 6(a) and Fig. 6(b), respectively, display examples of contours of the calculated minor principal stress and major principal stress. In these examples, R_c, T, d, θ_1, θ_2 respectively denote the quantities of 214 mm, 8 mm, 12.8 mm, 26°, and 38°. Stress concentrations of minor principal stress appear at the inner edge of the through-hole (Point A, peak value is -1,740 MPa) and at the inner foot of the reinforcement (Point B, peak value is -1,760 MPa). The level of the major principal stress is much lower than

the tensile strength of 726 MPa. Its effect on the pressure tolerance of the vessel is negligible.

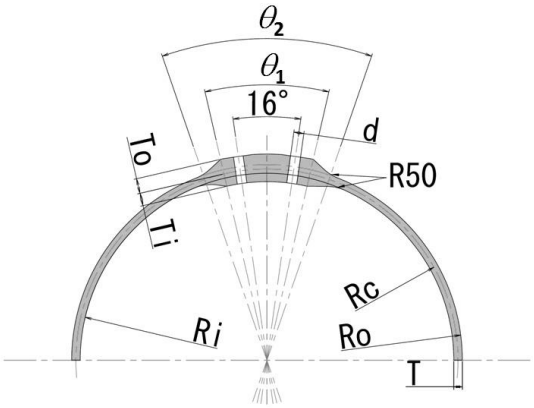

Fig. 5. Cross-section view of the model for FEM analysis for silicon-nitride ceramic pressure-tight housing with 110 MPa withstand pressure (unit: mm).

R_i: Inner radius
R_c: Center radius
R_o: Outer radius
T: Thickness of the shell
T_i: Thickness of the inner reinforcement
T_o: Thickness of the outer reinforcement
d: Diameter of the through-hole
θ_1, θ_2: Span of the reinforcement

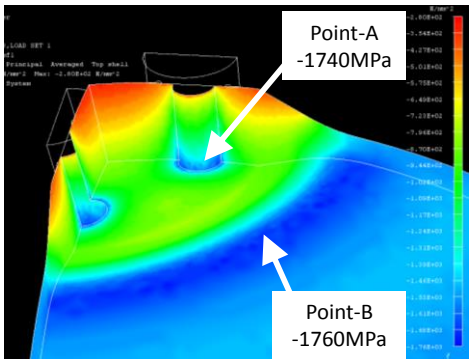

Fig. 6(a). Example of contour of the calculated minor principal stress.

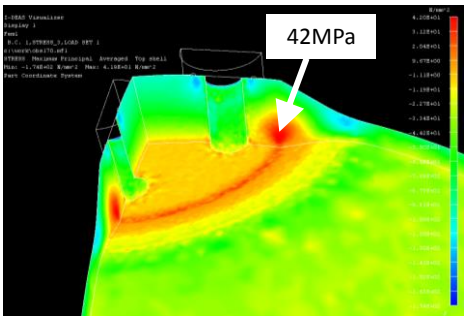

Fig. 6(b). Example of contour of the calculated major principal stress.

It can also be confirmed that practically no interference occurs between adjacent through-holes.

The hoop stress $\sigma_\theta(r)$ on the thin sphere at radius r can be expressed as shown below.

$$\sigma_\theta(r) = -\frac{P_o {R_O}^3}{{R_O}^3 - {R_i}^3}\left(1 + \frac{{R_i}^3}{2r^3}\right) \quad (1)$$

Therein, R_i, R_o, r, and P_o respectively denote the inner radius, outer radius, radius, and hydraulic pressure. Using (1), the hoop stress at the inner surface of the sphere is calculable as -1,555 MPa, which fairly coincides with the result of the FEM analysis of -1,560 MPa. This coincidence underscores the validity of the FEM analysis. Using this hoop stress, we can define a stress concentration coefficient σ_n, as the ratio between the peak value of the minor stress around portion and the hoop stress at the inner surface of the sphere $\sigma_\theta(R_i)$. We also respectively define σ_{nth} and σ_{nf} as the stress concentration coefficients at point A and at point B.

We analyzed a model with no reinforcement around through-holes. In this model, R_i, R_o, P_o, and d (diameter of through-holes) respectively represent 209 mm, 216.66 mm, 110 MPa, and 11.6 mm. The calculated normalized stress concentration σ_{nth} was 2.15. As described in the *Introduction*, two-fold stress concentration is known to appear around a through-hole on a thin infinite plane on which two orthogonal stresses parallel to the plane are added. The level of stress concentration around the through-hole on a pressure-tight sphere is similar to that of the case of a through-hole on a thin infinite plane.

Comparing these results of FEM analysis clarifies that, using proper reinforcement around through-holes, the level of the stress concentrations can be lowered at point A.

However, the reinforcement generates another stress concentration at point B, which implies that some proper level of reinforcement exists.

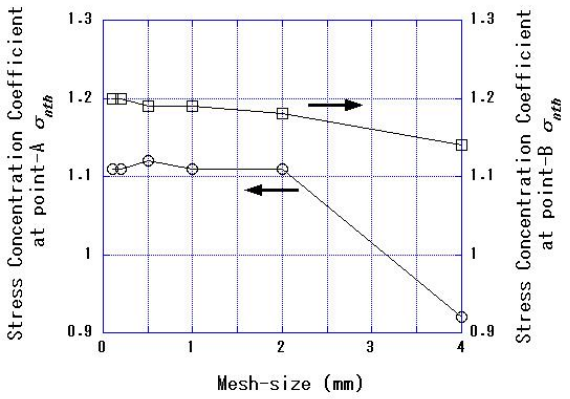

Fig. 7. Mesh-size effect on stress concentrations.

B. Effect of mesh size

Mesh size affects the level of calculated stress concentration. To evaluate this effect, we have analyzed the same model using mesh of several sizes, and compared them. Fig. 7 portrays the relation between the mesh size and the calculated stress concentration at point A and at point B. In this model, R_i, R_o, P_o, and d are, respectively, 213.12 mm, 222.88 mm, 110 MPa and 12.8 mm. The mesh size is less than 0.5 mm. Smaller meshes were used only around point A and point B because of the limitation of computer resources. Variation of the stress concentration coefficient is smaller in a range for mesh smaller than 2 mm (variations are less than $\pm 0.5\%$ for point-A and $\pm 0.8\%$ for point-B in this range.) Therefore, we have generally used mesh sizes of 1 mm around point A and point B for FEM analyses.

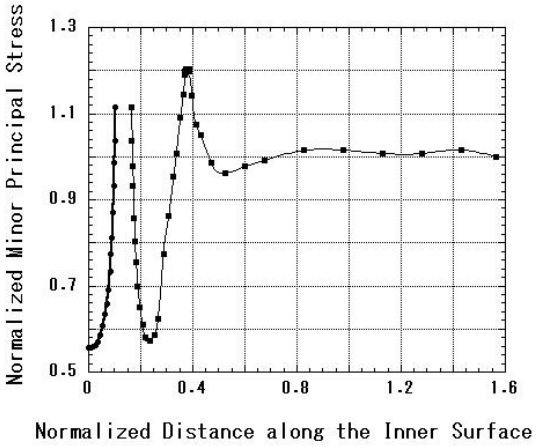

Fig. 8. Variation of the minor principal stress along the inner surface of the hemisphere. The horizontal axis shows the distance from the top of the hemisphere being measured along the inner surface. It is normalized by the inner radius of the hemisphere.

Fig. 8 depicts the variation of the minor principal stress along the inner surface of the hemisphere. The mesh sizes in this analysis are 0.1 mm around point A and point B. Other parameters are the same as those shown for Fig. 7.

C. Proper combination of the inner thickness and outer thickness of the reinforcement

We sought the proper shape of the reinforcement to assure that both stress concentration levels at point A and at point B are lower than the desired level. Three primary parameters were chosen to describe the reinforcement shape: thickness of the inner reinforcement T_i, thickness of the outer reinforcement T_o, and thickness of the shell T, as presented in Fig. 5. The normalized thicknesses of the inner and the outer reinforcement t_i and t_o were defined as shown below.

$$t_i = \frac{T_i}{T} \tag{2}$$

$$t_o = \frac{T_o}{T} \tag{3}$$

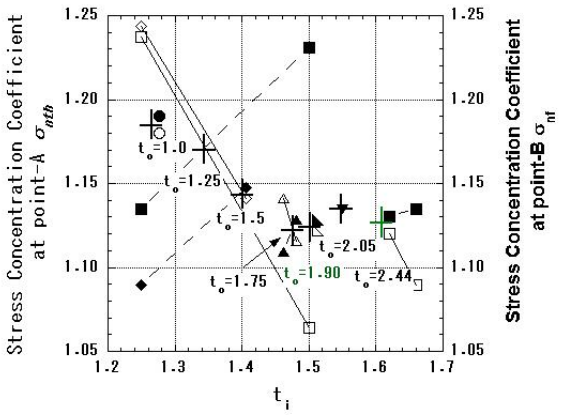

Fig. 9. Relation between thickness of reinforcement t_i/t_o and stress coefficients at point A σ_{nth} and at point B σ_{nf}.

We conducted FEM analyses using several combinations of t_i and t_o. In these analyses, R_i, R_o, P_o, and d respectively denote 210 mm, 218 mm, 110 MPa and 12.8 mm. Fig. 9 portrays some examples of results, where straight lines and dashed lines show a set of data that have the same t_o. Straight lines link stress concentrations at point A, and dashed lines link stress concentrations at point B. When t_i increases, stress concentration coefficients σ_{nth} at point A decrease, whereas stress concentration coefficients at point B σ_{nf} increase. There exist some t_i corresponding to each t_o with which both stress concentration coefficients σ_{nth} and σ_{nf} become mutually equivalent, namely

$\sigma_{nth} := \sigma_{nf} := \sigma_n$. These points are represented by cross-shapes in Fig. 9. It is clear from Fig. 9 that a series of proper combinations of t_i and t_o exists.

Fig. 10 shows proper combinations of t_i and t_o and their relation. Some additional points shown in Table 2 are added to the points shown in Fig. 9. The proper combinations of t_i and t_o share a mutually linear relation in the calculated region. In this case, the relation can be described as follows.

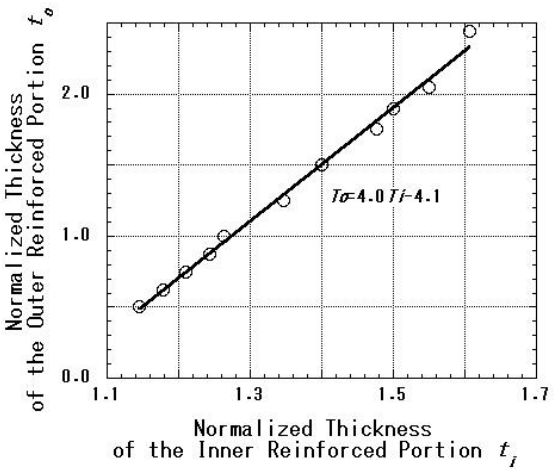

Fig. 10. Relation between t_i and t_o of proper combinations.

$$t_o = 4.0t_i - 4.1 \qquad (4)$$

Although this relation depends on other parameters such as hemisphere thickness, the through-hole diameter, and the shape of the reinforcement, we will later show that these dependences are not so large.

Table 2 Additional calculated points

ti	to	σ_{nth} (MPa)	σ_{nf} (MPa)
1.145	0.599	-2250	-2280
1.178	0.625	-2080	-2140
1.210	0.750	-1950	-2020
1.243	0.875	-1860	-1910
1.510	1.900	-1750	-1760
1.550	2.050	-1770	-1770

D. Limitation of the reduction of the stress concentration

Fig. 11 presents the relation between the normalized total thickness of the reinforcement $t_a = t_i + t_o$ and the stress concentration coefficient σ_n. This figure

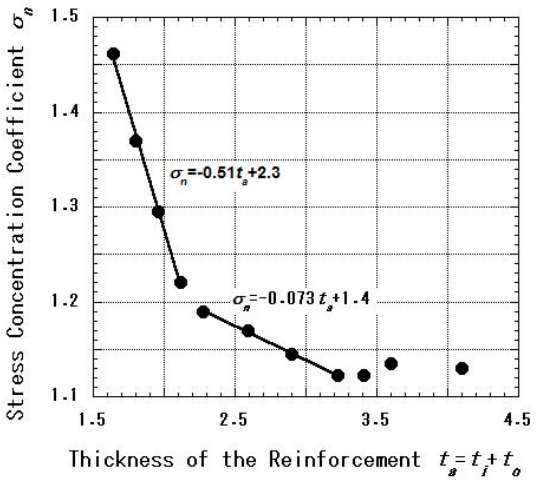

Fig. 11. Relation between the thickness of reinforcement t_i+t_o and the stress concentration coefficient σ_n.

shows that the normalized stress concentration σ_n decreases concomitantly with increasing t_a in the region of smaller t_a, but the rate of decrease declines and finally stops. Results show that the lower limit of the reduction of the stress concentration is about 1.12.

E. Effect of other parameters and misalignment between two hemispheres

Some other parameters affect the stress concentration: the hemisphere thickness, the through-hole radius, and the width of the reinforcement and the fillet. Table 3 presents these effects. The other parameters, R_c (center radius), t_i, t_o, and hydraulic pressure, are 214 mm, 1.481, 1.750, and 110 MPa, respectively. Effects of variation of parameters are less than 7% in the calculated range.

Misalignment between two hemispheres causes another stress concentration at the jointing portion. Fig. 12 portrays the contour of the minor principal stress and its enlarged view around the jointing portion.

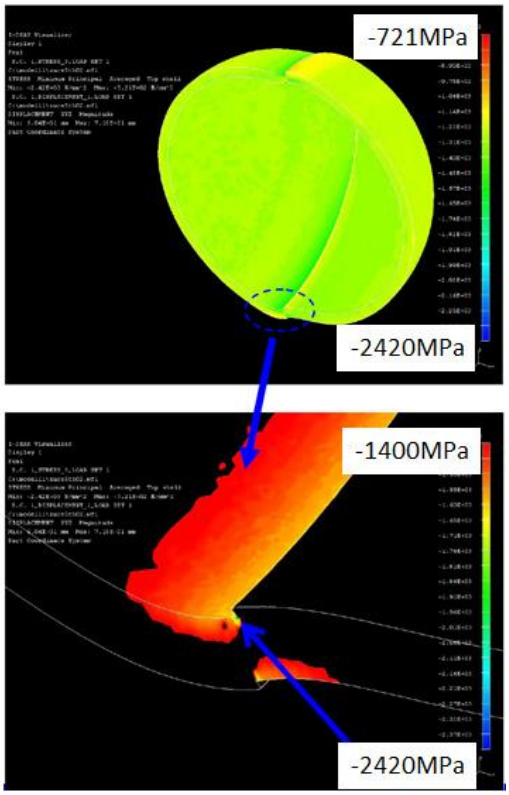

Fig. 12. Contour of the minor principal stress caused by misalignment between two hemispheres and its enlarged view.

In this analysis, R_i, R_o, and P_o are, respectively, 213.12 mm, 222.88 mm, and 110 MPa. Misalignment of 0.976 mm, that is about 10% of the shell thickness, is assumed. We arranged chambers of 0.1 mm at edges of hemispheres. The material is silicon-nitride ceramic. No through-hole exists on the hemispheres. The white line shows the enlarged deformation. Some stress concentrations appear at corners of hemispheres. The maximum value of the minor principal stress is -2,420 MPa, which is 1.84 times the theoretical hoop stress at the inner surface of the hemisphere. Table 4 presents the

relation between the misalignment and the stress concentration coefficient of the minor and major principal stress. It is clear that both stress concentration of the major principal stress and the minor principal stress are significant in the case of misalignment. We should minimize the misalignment.

Table 3 Effect of other parameters

	Thickness of hemisphere (mm)	Diameter of through-holes (mm)	Span of reinforcement	Fillet (mm)	Normalized stress concentration at Point A	Normalized stress concentration at Point **B**
Standard	8	12.8	26°–38°	50	1.12	1.13
Thickness of hemisphere	4	12.8	26°–38°	50	1.07	1.10
	6	12.8	26°–38°	50	1.11	1.13
	10	12.8	26°–38°	50	1.14	1.21
Diameter of through-holes	8	6.4	26°–38°	50	1.15	1.14
	8	12.8	26°–38°	50	1.15	1.15
	8	19.2	26°–38°	50	1.18	1.10
Span of reinforcement	8	19.2	26°–33.5°	50	1.13	1.19
Fillet	8	12.8	26°–38°	0	1.12	1.59

Table 4 Stress concentration attributable to misalignment between two hemispheres

Amount of misalignment (percentage of shell thickness)	Stress concentration	Maximum minor principal stress (MPa)
0	1.11	37
1	1.18	157
4	1.47	299
10	1.84	436
20	2.09	303

III. Design Criteria of Ceramic Pressure-tight Housings for OBS and Hydraulic Pressure Tests

A. Design criteria of ceramic pressure-tight housings

When choosing the design criteria and safety factor, we assign priority to reliability. Therefore, we adopted a safety factor of 2, except for stresses caused by the misalignment, which means the peak value of the concentrated minor stress should be equal to or lower than half of the compressive strength.

B. Hydraulic pressure test

To date, we have produced small pressure-tight housings of silicon-nitride ceramics (Fig. 3), a real housing of silicon-nitride ceramic for 11 km OBS (Fig. 4) and small pressure-tight housings of alumina ceramics. Table 5 presents the principal figures of these housings. Using these housings, we conducted a series of hydraulic pressure tests. Careful attention was devoted to avoidance of misalignment between the two hemispheres. Table 6(a), Table 6(b) and Table 6(c) summarize these hydraulic pressure tests. The period of the cyclic hydraulic pressure tests was about 5–6 min. The break-down hydraulic pressure of the small pressure housing of alumina ceramic was 164 MPa. Considering the rated hydraulic pressure of 80 MPa and the safety factor of 2, it is a quite reasonable break-down pressure. The highest hydraulic pressure that the

small silicon-nitride ceramic housings were subjected to was 172 MPa. This was the highest hydraulic pressure that the test tank was able to generate. Results of these hydraulic pressure tests demonstrate the validity of the proposed design method.

Table 5 Principal figures of the produced ceramic pressure-tight housings

	Material	Maximum Pressure	Safety Factor	R_i	R_o	t_i	t_o	d	θ
		MPa		mm	mm			mm	deg
Small model-1	Silicon-nitride	110	2	53.28	55.72	1.48	1.75	3.2	26–38
11,000, OBS	Silicon-nitride	110	2	213.12	222.88	1.48	1.75	11.45/11.05	26–38
Small model-2	Alumina	80	2	52.94	55.72	1.48	1.75	8	26–38

Table 6(a) Hydraulic pressure test of the small model-1 of ceramic pressure housing for 11 km OBS

Item	Hydraulic Pressure	Duration	Number of cycles
	MPa	hour	
Long Term Pressurization	120	1,224	-
Repeated Pressurization – 1	110	-	300
Repeated Pressurization – 2	130	-	30
Short Term Pressurization	172	-	-

Table 6(b) Long-term hydraulic pressure tests of the small model-2 of alumina ceramic pressure housing

Item	Pressure	Duration	Number of cycles
	MPa	hh:mm	
Pressurization – 1	80	155:25	-
Pressurization – 2	88	65:11	-
Pressurization – 3	96	182:13	-
Pressurization – 4	104	27:40	-
Pressurization – 5	112	16:54	-
Pressurization – 6	120	167:27	-
Pressurization – 7	130	00:10	-
Pressurization – 8	136	00:25	-
Pressurization – 9	144	00:05	-
Pressurization – 10	152	00:18	-
Pressurization – 11	164	Break-down	-
Repeated Pressurization – 1	88	-	257
Repeated Pressurization – 3	96	-	25
Repeated Pressurization – 4	104	-	50
Repeated Pressurization – 5	112	-	68
Repeated Pressurization – 6	120	-	208

Table 6(c) Hydraulic pressure test of the ceramic pressure housing for 11 km OBS

Item	Hydraulic Pressure	Duration	Number of cycles
	MPa	hour	
Pressurization	110	1	-

IV. CONCLUDING REMARKS

Ceramics provide higher compressive strength and lower specific gravity than those of typical metals. Making good use of these features, we can produce light pressure-tight housings that have good durability and sufficient buoyancy up to 11 km water depth.

As described in this paper, we presented the design method for ceramic pressure-tight housings for OBSs. We also presented the detailed technical background of the design method. After conducting a series of FEM analyses, we examined the results, which revealed a certain regularity between the thickness of the reinforcement and the stress concentration. This regularity is useful to design the reinforcement around the through-hole on the ceramic pressure-tight housing.

Based on FEM analysis results, we developed (a) small models of silicon-nitride ceramic pressure-tight housings for OBSs, (b) actual-sized silicon-nitride ceramic pressure-tight housing, and (c) small models of alumina ceramic pressure tight housings. Results of hydraulic pressure tests obtained using these housings demonstrated the

validity of the design method. We are now developing an OBS that is operational at 11 km water depth using the silicon-nitride ceramic pressure-tight housing.

We chose a safety factor of 2, which might seem inappropriately high as a safety factor. However, little information is available on the mechanical characteristics of ceramics against compressive strength: we have limited information related to volume dependence of compressive strength, mechanics of break-down caused by stress concentration, effect of cyclic pressurization, etc. Information related to this matter is slight because, in most ceramic structures, their strength is limited by the tensile strength: it is much lower than the compressive strength. We need not devote much attention to the compressive strength in most applications. We believe that finding the proper safety factor remains another issue to be addressed.

ACKNOWLEDGMENTS

We would like to express our heartful gratitude to Prof. Shinichi Takagawa of The University of Tokyo, Mr. Hideyuki Murakami of Kaiyo Denshi Co., Ltd., Mr. Yoshihiro Aiba and Kakuichi Tomimoto of Kyocera Corporation and Mr. Hiroyasu Momma of Nippon Marine Enterprises, Ltd. for their fruitful discussion and encouragement.

REFERENCES

[1] J. D. Stachiw, D. Peters and G. McDonald, "Ceramic External Pressure Housings for Deep Sea Vehicle J. Clerk Maxwell," in Proc. OCEANS'06 MTS/IEEE Boston, 2006.

[2] S. Weston, J. Stachiw, R. Merewether, M. Olsson and G. Jemmott, "Alumina Ceramic 3.6in Floatation Spheres for 11 km ROV/AUV Systems," in Proc. OCEANS'05 MTS/IEEE Washington, 2005.

[3] J. D. Stachiw and Donald Peters, "Alumina Ceramic 10in Floatation Spheres for Deep Submergence ROV/AUV Systems," in Proc. OCEANS'05 MTS/IEEE Washington, 2005.

[4] A. D. Bowen, D. R. Yoerger, C. Taylor, R. McCabe, J. Howland, D. Gomez-Ibanez, J. C. Kinsey, M. Heintz, G. McDonald, D. B. Peters, B. Fletcher, C. Young, J. Buescher, L. L. Whitcomb, S. C. Martin, S. E. Webster and M. V. Jakuba, "The Nereus Hybrid Underwater Robotic Vehicle for Global Ocean Science Operations to 11,000 m Depth," in Proc. OCEANS'08 MTS/IEEE Quebec, 2008.

[5] Y. Yano and S. Takagawa, "Study on Spherical Pressure Vessel of Ceramics for Deep-sea Buoyancy Module Applications," proc. of OCEANS'04 MTS/IEEE/TECHNO-OCEAN'04, 2004.

[6] Y. Yano and S. Takagawa, "Exploratory Study on Engineering Ceramics Pressure Hulls for Deep-Sea Submergence Services," Marine Technology Society Journal, vol. 39, num. 3, pp.49-55, 2005.

[7] K. Asakawa, M. Ito and T. Hyakudome, "Evaluation of Small Models of Ceramic Housings for 11,000 m Ocean Bottom Seismometers," in Proc. of OCEANS'10 IEEE Sydney, 2010.

[8] K. Baba, M. Ito, H. Tanaka, and H. Momma, “Advanced Operation of Ocean Bottom Seismometer,” in Proc. of The Thirteenth (2003) International Offshore and Polar Engineering Conference Honolul, pp.228-230, 2003.

[9] K. Asakawa, T. Hyakudome, M. Yoshida, and N. Ookubo, “Development of Small-sized Models of Low-cost Alumina Ceramic Pressure-tight Housings for Ocean-bottom Seismometers,” in Proc. of Symposium on Underwater Technology 2011 and Workshop on Scientific Use of Submarine Cables & Related Technologies 2011, 2011.

Biographies

Kenichi Asakawa received the B.E., M.S., and Dr. Eng. degrees in engineering from Tokyo Institute of Technology, Tokyo, Japan, in 1974, 1976, and 1979, respectively.
He joined KDD Research and Development Laboratories in 1979 where he had been engaged in developments of ROVs, AUVs, and other technologies related to construction and maintenance of underwater telecommunication cables. In 2002, he moved to the Japan Agency for Marine-Earth Science and Technology (JAMSTEC, formerly, Japan Marine Science and Technology Center), Yokosuka, Japan. Since then he has been involved in the development of ocean observing systems and related technologies.

Tadahiro Hyakudome received the D.E. degrees in marine engineering from Kyushu University, Japan, in 2000. In 2000, he joined Japan Agency for Marine-earth Science and Technology (JAMSTEC). He belongs to research group on Advanced Autonomous Underwater Vehicle. His current research interests include underwater vehicle, material, power system, vehicle shape and launch system.

Masao Yoshida received the B.E. and M.E. degrees in engineering from Himeji Institute of Technology, Hyogo, Japan, in 1994 and 1996, respectively.
He joined KYOCERA, Kagoshima, Japan, in 1996, Since then he has been engaged in the production technology of ceramics, especially in the design of industrial ceramic devises using finite-element analysis.

Naoyuki Okubo received the B.E. degrees in industrial chemistry from University of Miyazaki, Miyazaki, Japan, in 1990.

He joined KYOCERA, Kagoshima, Japan, in 1990, and since then he has been engaged in the production technology of industrial ceramic devises and ceramic articles for environmental application.

Makoto Ito received the Master of Engineering in Electrical Engineering from SHONAN INSTITUTE OF TECHNOLOGY, Kanagawa, Japan, in 1997.
He joined Nippon Marine Enterprises, Ltd. YOKOSUKA, Japan, in 1997. Since then he has been engaged in marine geophysical surveys and observations using multichannel seismic reflection survey systems, single-channel seismic reflection survey systems, ocean bottom seismometers and other instruments.

Ikumasa Terada received the Bachelor of Fishery degrees in physical oceanography from Kagoshima University, Kagoshima, Japan, in 2000.
He joined Nippon Marine Enterprises, Ltd. YOKOSUKA, Japan, in 2000. Since then he has been engaged in marine geophysical surveys and observations using multichannel seismic reflection survey systems, single-channel seismic reflection survey systems, ocean bottom seismometers and other instruments.

Authors

Kenichi Asakawa	Japan Agency for Marine-Earth Science and Technology
	asakawa@jamstec.go.jp, tel +81-46-867-9311
Tadahiro Hyakudome	Japan Agency for Marine-Earth Science and Technology
Masao Yoshida	Kyocera Corporation
Naoyuki Okubo	Kyocera Corporation
Makoto Ito	Japan Agency for Marine-Earth Science and Technology
Ikumasa Terada	Nippon Marine Enterprises, Ltd.

Japan Agency for Marine-Earth Science and Technology
2-15 Natsushima-cho
Yokosuka 237-0061 Japan